Spatial control of spontaneous parametric down-conversion photon pairs through the use of apertured Bessel-Gauss pump beams

Dalia Gutiérrez-López, Mónica Maldonado-Terrón, R. Josué Hernández, Verónica Vicuña-Hernández, Roberto Ramírez-Alarcón, Héctor Cruz-Ramírez, Rocío Jáuregui, and Alfred B. U'Ren

Phys. Rev. A **100**, 013802 — Published 2 July 2019

DOI: 10.1103/PhysRevA.100.013802

Spatial control of spontaneous parametric down-conversion photon pairs through the use of apertured Bessel-Gauss pump beams

Dalia Gutiérrez-López,[1] Mónica Maldonado-Terrón,[1] R. Josué Hernández,[2] Verónica Vicuña-Hernández,[3] Roberto Ramírez-Alarcón,[4] Héctor Cruz-Ramírez,[1] Rocío Jáuregui,[5,*] and Alfred B. U'Ren[1,†]

[1] *Instituto de Ciencias Nucleares, Universidad Nacional Autónoma de México, Apdo. Postal 70-543, 04510 Cd. de México, México*

[2] *Cátedra CONACYT Consejo Nacional de Ciencia y Tecnología - Instituto de Ciencias Nucleares, Universidad Nacional Autónoma de México, Apdo. Postal 70-543, 04510 Cd. de México, México*

[3] *ICFO-Institut de Ciencies Fotoniques, Mediterranean Technology Park, 08860 Castelldefels (Barcelona), Spain*

[4] *Centro de Investigaciones en Óptica A.C., Loma del Bosque 115, Colonia Lomas del Campestre, 37150 León Guanajuato, México*

[5] *Instituto de Física, Universidad Nacional Autónoma de México, Apdo. Postal 20-364, 01000 Cd. de México, México*

(Dated: June 5, 2019)

We demonstrate, both experimentally and theoretically, a method that allows us to modify the spatial properties of photon pairs produced by the process of spontaneous parametric down-conversion (SPDC) with an apertured, zeroth-order Bessel-Gauss beam. Concentrating on the use of a half-plane aperture, we show that the phasematching conditions for non-paraxial pump beams can be controlled by simply changing the aperture orientation. Partially blocking the pump beam, leads to a selection of either one of two individual cones that form a dual-cone SPDC angular spectrum, or a portion of both of them. We can likewise determine the shape and orientation of the conditional angular spectrum. This control of the SPDC spatial properties could be useful for quantum information processing protocols.

PACS numbers: 42.50.-p, 42.50.Dv, 03.65.Ud

I. INTRODUCTION

The generation of custom light fields with structured intensity, polarization and phase is currently an exciting field of research with multiple applications [1–3]. In particular, spatially structured light can be employed in the quantum realm *e.g.* for large-alphabet quantum key distribution [4], microscopy with super-resolution [5], and quantum crystalography [6].

In this work we contribute to the exploration of non-classical structured light through a careful study, of the spatial properties of co-polarized (type-I) SPDC photon pairs, produced by a pump in the form of an apertured beam. We focus our attention on Bessel-Gauss beams since they exhibit some remarkable properties including i) propagation invariance [7], ii) self-healing [8, 9], iii) resistance to deformation in transmission through a turbulent medium [10, 11], and iv) the presence of orbital angular momentum for higher-order modes. The question of how these properties can play a role for photon pairs and heralded single photons is an ongoing research topic. Postselection configurations can be employed in order to study entanglement and correlations in photon pairs in the OAM degree of freedom by decomposing the two photon state using certain families of modes as basis, such as Laguerre-Gauss [12, 13] and Bessel-Gauss [14]. In this case the pump beam need not be spatially structured; in particular, it can be in the form of a standard Gaussian beam. A second approach corresponds to the use of a shaped pump with a transverse structure that already possesses properties such as i)-iv) so as to confer similar properties to the heralded single photons. In our own work, we have demonstrated the transfer of non-diffractive behavior [15], on the one hand, and OAM [16], on the other hand, from the pump beam in the SPDC process to heralded single photons.

A standard zeroth-order Bessel-Gauss (BG) beam is characterized by two parameters: the radius of the angular spectrum in transverse wavevector space $\kappa_\perp$ and its width $\delta_{\kappa_\perp}$. It is known [16–18] that these structured beams with a sufficiently large value of $\kappa_\perp$, i. e., beyond the paraxial approximation and with $\kappa_\perp \gg \delta_{\kappa_\perp}$, lead to a SPDC angular spectrum formed by two non-concentric cones. This contrasts with the opposite case $\kappa_\perp \ll \delta_{\kappa_\perp}$ (including the Gaussian-beam case $\kappa_\perp \to 0$) for which the angular spectrum consists of a single cone [17–21]. The location of the two cones is asymmetric, as mediated by the pump walk-off and the asymmetric distribution of the wavevectors in the incoming Bessel pump beam with respect to the optic axis. One cone contains the other in such a manner that the two meet tangentially [17]. In [22] we explored how this dual cone structure leads to double transverse wavevector correlations.

Here we investigate how the spatial SPDC properties can be controlled by a binary aperture so as to restrict the pump angular spectrum, that is, its transverse wavevector composition. We show theoretically and through ex-

* rocio@fisica.unam.mx

† alfred.uren@correo.nucleares.unam.mx

perimental measurements that, placing a half-plane obstruction, it becomes possible to select the outer (inner) SPDC cone when blocking the top (bottom) half of the pump angular spectrum. When the half plane obstruction is configured at any other orientation, a portion of both cones remains. In this manner, an experimenter close to the source, can determine through the orientation of the obstruction, the resulting angular emission properties of the photon pairs.

II. ANGULAR SPECTRUM

A directly measurable property of SPDC photon pairs is their angular spectrum (AS). It corresponds to the spatially-resolved, single-photon rate of detection in the transverse wavevector domain. It can be calculated as

$$R_s(\mathbf{k}^{\rm s}_\perp) = |g\alpha_p|^2 \int {\rm d}\omega^{\rm s} \cdot \int {\rm d}^2 k^{\rm i}_\perp |F(\mathbf{k}^{\rm s}_\perp, \omega^{\rm s}, \mathbf{k}^{\rm i}_\perp, \omega^{\rm p}-\omega^{\rm s})|^2, \tag{1}$$

where g is an effective coupling constant that incorporates the $\chi^{(2)}$ nonlinearity of the crystal, and α_p is the coherent-state amplitude of the pump beam [22]. In this equation the joint amplitude $F(\mathbf{k}^{\rm s}_\perp, \omega^{\rm s}, \mathbf{k}^{\rm i}_\perp, \omega^{\rm p}-\omega^{\rm s})$ depends on the structure of the incident pump beam through its angular spectrum $\psi(\mathbf{k}^{\rm p}_\perp)$, and can be expressed as

$$F(\mathbf{k}^{\rm s}_\perp, \omega^{\rm s}, \mathbf{k}^{\rm i}_\perp, \omega^{\rm p}-\omega^{\rm s}) = \psi(\mathbf{k}^{\rm s}_\perp + \mathbf{k}^{\rm i}_\perp)\, {\rm sinc}(L\,\Delta k_z/2)\exp(-i\,L\,\Delta k_z/2). \tag{2}$$

This equation takes into account the strong phase matching conditions $\mathbf{k}^{\rm p}_\perp = \mathbf{k}^{\rm s}_\perp + \mathbf{k}^{\rm i}_\perp$ valid for a wide (as compared to the pump transverse dimensions) nonlinear crystal, as well as the effect of the much shorter crystal length L; $\Delta k_z = k^{\rm p}_z - k^{\rm s}_z - k^{\rm i}_z$ represents the phase mismatch, and the signal (idler) wavevectors are evaluated at frequencies $\omega^{\rm s}$ ($\omega^{\rm p}-\omega^{\rm s}$). For a linearly-polarized zeroth-order Bessel-Gauss beam, the angular spectrum corresponds to a Gaussian function of the modulus of the transverse component of the wavevector around a given value $\kappa_\perp$ of width $\delta_{\kappa_\perp}$,

$$\psi(\mathbf{k}^{\rm p}_\perp) = {\rm e}^{-(k^{\rm p}_\perp - \kappa_\perp)^2/2\delta^2_{\kappa_\perp}}. \tag{3}$$

Note that Eq. (3) reduces to the angular spectrum of a Gaussian beam for $\kappa_\perp \ll \delta_{\kappa_\perp}$. Here we are interested in the opposite regime: $\kappa_\perp \gg \delta_{\kappa_\perp}$. For such a beam, quasi propagation-invariance can be taken as guaranteed, while it gives a closer approximation to realistic beams that can be implemented in the laboratory, as compared to the ideal Bessel beams for which $\delta_{\kappa_\perp} = 0$. Note, however, that in actual realizations of Bessel-like beams, the Gaussian structure may be replaced by other single-peaked distributions.

Frequency-degenerate SPDC (i.e. with $\omega^{\rm s} = \omega^{\rm i} = \omega^{\rm p}/2$), for a BG pump beam, leads to the following expression for the angular spectrum $R_s(\mathbf{k}_\perp)$, evaluated at the signal transverse wavevector $\mathbf{k}^{\rm s}_\perp = (\mathrm{k}^{\rm s}_x, \mathrm{k}^{\rm s}_y)$ [17]

$$R_s(\mathbf{k}^{\rm s}_\perp) \approx {\rm e}^{-\sigma^{-2}_{\rm AS}\left((\mathrm{k}^{\rm s}_\perp)^2 - r^2_{\rm AS}\right)^2} \times \int_0^{2\pi} {\rm e}^{-\frac{(\gamma L)^2}{2}(|\mathbf{d}|\kappa_\perp \sin\varphi_p - \tilde\kappa)^2} d\varphi_p, \tag{4}$$

where the integration variable φ_p represents the azimuthal angle in the pump beam angular spectrum. In Eq. (4) the following notation is used,

$$r^2_{\rm AS} = (1/2)\left(\mathrm{n_o}\omega^{\rm p}/c\right)^2 (1 - (\mathrm{n_e}/\mathrm{n_o}))\,, \tag{5}$$

$$\sigma^{-2}_{\rm AS} = 2(\gamma L c/\mathrm{n_o}\omega^{\rm p})^2, \tag{6}$$

$$\tilde\kappa = (\omega^{\rm p}/c)(\mathrm{n_e} - \mathrm{n_o}) + (2c/\mathrm{n_o}\omega^{\rm p})(\mathrm{k}^{\rm s}_\perp)^2, \tag{7}$$

and

$$\mathbf{d} = \beta \mathbf{a}_\perp + (2c/\mathrm{n_o}\omega^{\rm p})\mathbf{k}^{\rm s}_\perp. \tag{8}$$

These expressions rely on a Gaussian approximation for the sinc function, ${\rm sinc}(x) \approx \exp[-(\gamma x)^2]$ with $\gamma = 0.4393$. $\omega^{\rm p}$ represents the pump frequency, n_e (n_o) is the extraordinary-ray (ordinary-ray) refractive index at the degenerate SPDC frequency, while β is a measure of the so-called Poynting vector walk-off; $\mathbf{a}_\perp$ represents the projection on the transverse plane of a unitary vector parallel to the optic axis. Equation (4) incorporates first order corrections to the paraxial expression of the dispersion relations for a light beam that impinges upon the crystal in the normal direction.

Note that for a negative uniaxial crystal ($\mathrm{n_e} < \mathrm{n_o}$) and for a paraxial pump beam, i. e. $\kappa_\perp \ll (\omega^{\rm p}/c)|\mathrm{n_e} - \mathrm{n_o}|$, (which includes Gaussian-beam pumps with $\kappa_\perp \to 0$ as a special case), the AS is concentrated nearby a cone given by the condition [23]

$$k^{\rm s}_\perp = (\mathrm{n_o}\omega^{\rm p}/\sqrt{2}c)\sqrt{1 - \mathrm{n_e}/\mathrm{n_o}} = r_{\rm AS}. \tag{9}$$

As $\kappa_\perp$ increases, the restriction $k^{\rm s}_\perp \approx r_{\rm AS}$ is relaxed: the SPDC spatial structure is the result of the superposition of the contributions to the two-photon state from individual pump wavevectors that arrive symmetrically on the crystal front surface, but are not distributed symmetrically with respect to the optic axis. This anisotropy produces structures that are not centered at the origin, but are displaced along the direction of the optic axis. This displacement is absent for $\kappa_\perp \to 0$, e.g. for a Gaussian-beam pump. The AS of a Bessel-Gauss beam which is outside the paraxial regime involves two non-homogenous (i.e. with an azimuthally-varying width) and non-concentric cones with unequal

radii [17]. For a negative birefringent crystal and for $|\mathrm{n_o}\omega^{\mathrm{p}}\beta\mathbf{a}_\perp/2c| \approx r_{\mathrm{AS}} \gg \kappa_\perp$, the two cones have a quasi-circular transverse structure with larger (smaller) radii r_+ (r_-), and centers defined by the transverse vectors $A_+\hat{\mathbf{a}}_\perp$ ($A_-\hat{\mathbf{a}}_\perp$), with

$$r_\pm \approx r_{\mathrm{AS}} - \frac{\kappa_\perp}{2}\Big(1 \pm \frac{\mathrm{n_o}\omega^{\mathrm{p}}\beta|\mathbf{a}_\perp|}{2cr_{\mathrm{AS}}} \mp \frac{\kappa_\perp}{2r_{\mathrm{AS}}}\Big), \quad (10)$$

$$A_\pm \approx \mp\frac{\kappa_\perp}{2}\Big(1 + \frac{\mathrm{n_o}\omega^{\mathrm{p}}\beta|\mathbf{a}_\perp|}{2cr_{\mathrm{AS}}} - \frac{\kappa_\perp}{2r_{\mathrm{AS}}}\Big). \quad (11)$$

The two emission cones are nearly tangent to each other along the direction defined by the wavevector $\sim (-r_{\mathrm{AS}} + \kappa_\perp/2)\hat{\mathbf{a}}_\perp + k_z\hat{e}_z$. The double conical structure of the AS reflects both the asymmetric distribution of the wavevectors in the incoming Bessel pump beam with respect to the optic axis and effects proportional to the β term arising in the extraordinary-ray dispersion relation.

These properties of the AS for a BG pump beam have been corroborated experimentally [22]. An interesting consequence of the resulting pair of non-homogenous and non-concentric emission cones is the appearance of double transverse wavevector correlations. In the present manuscript, we are interested in the possibility of controlling the dual cone structure by restricting the transverse intensity of the pump through the placement of a binary mask in the transverse wavevector domain. For BG beams such an aperture limits the possible values of the azimuthal angle which defines the orientation of the wavevector φ_p. We are particularly interested in restricting the pump angular spectra as $\varphi_o \le \varphi_p \le \varphi_F$, that is, corresponding to a circular sector of the transverse plane, centered on the pump axis. In such a case, the AS is given by

$$\tilde{R}_s(\mathrm{k}^{\mathrm{s}}_x, \mathrm{k}^{\mathrm{s}}_y; \varphi_0, \varphi_F) \approx \mathrm{e}^{-\sigma_{\mathrm{AS}}^{-2}\left((\mathrm{k}^{\mathrm{s}}_\perp)^2 - r_{\mathrm{AS}}^2\right)^2} \times \int_{\varphi_0}^{\varphi_F} \mathrm{e}^{-\frac{(\gamma L)^2}{2}(|\mathbf{d}|\kappa_\perp \sin\varphi_p - \tilde{\kappa})^2} d\varphi_p. \quad (12)$$

Since $\kappa_\perp$ appears in the integrand specifically as $\kappa_\perp \sin\varphi_p$, depending on the sign of the sine function in the exponent, the values of $\tilde{\kappa}$ over which the integral gives rise to significant values will be either positive (yielding larger values of $k_\perp$ with respect to r_{AS}) or negative (yielding lower values of $k_\perp$ with respect to r_{AS}). From these considerations, we would expect that restricting the pump angular spectrum as $0 < \varphi_p < \pi$ ($\pi < \varphi_p < 2\pi$) would guarantee that the bi-photon will be emitted nearby the external (internal) cone.

This is illustrated in Fig. 1 where panel (a) shows an experimental measurement of the SPDC AS for an unobstructued pump AS for specific values of $\kappa_\perp$ and $\delta_{\kappa_\perp}$ (see experimental Section). Panel (b) shows a corresponding simulation based on Eq. (13), making it clear that our numerical simulation agrees well with the experimental measurement. It is evident from the figure that the single-photon AS is composed of two rings, one external and one internal. Panel (c) shows the effect of

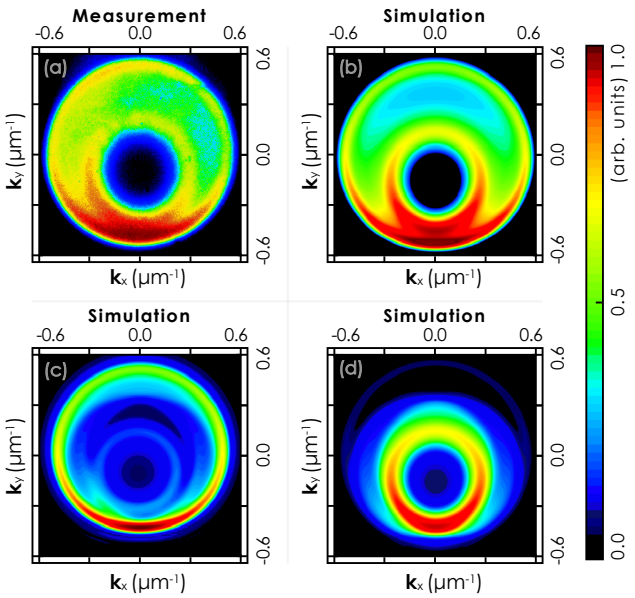

FIG. 1. (a) Measured angular spectrum for SPDC with an unobstructed (i.e. $0 \le \varphi_p < 2\pi$) Bessel-Gauss beam with $\kappa_\perp = 0.170\mu\mathrm{m}^{-1}$ and wavelength $\lambda = 405.5$nm. (b) Simulation corresponding to the experimental situation in (a). (c) and (d) show simulations similar to that presented in panel (b), with a half-plane obstruction characterized by $0 \le \varphi_p < \pi$ and $\pi \le \varphi_p < 2\pi$, respectively. Note that these simulations assume that only the frequency-degenerate photon pairs are retained.

restricting the pump angular spectrum to the angular range $0 < \varphi_p < \pi$ in our simulation, which corresponds to blocking the lower half of the pump angular spectrum; it becomes clear that in this case the resulting SPDC AS is limited to the external cone of the unobstructed AS. Panel (d) shows the effect of restricting the pump angular spectrum in our simulation to the angular range $\pi < \varphi_p < 2\pi$, which corresponds to blocking the upper half of the pump angular spectrum; in this case the resulting SPDC AS is limited to the internal cone of the unobstructed single-photon AS. We would expect that for other orientations of the half-plane obstruction, a portion of each of the internal and external cones would be visible in the AS. Thus, a fine control over the transverse wavector signal and idler intensity distributions can be achieved through a simple angular selection of the pump beam in the transverse wavevector space.

III. CONDITIONAL ANGULAR SPECTRUM

The conditional angular spectrum R_c represents the angular spectrum of the signal photon conditioned on the detection of an idler photon with wavevector $\mathbf{k}^{\mathrm{i}}_0$. For zeroth-order BG pump beams, R_c may be expressed as

$$R_c(\mathbf{k}^{\mathrm{s}}_\perp; \mathbf{k}^{\mathrm{i}}_{\perp 0}; \omega^{\mathrm{s}}, \omega^{\mathrm{i}}_0) =$$

$$|g\alpha_p|^2 \mathscr{S}(\mathbf{k}^{\rm s}_\perp, \mathbf{k}^{\rm i}_{\perp 0}) \cdot \mathscr{L}(\mathbf{k}^{\rm s}_\perp, \mathbf{k}^{\rm i}_{\perp 0}; \omega^{\rm s}, \omega^{\rm i}_0)\,, \tag{13}$$

with

$$\omega^{\rm s} + \omega^{\rm i}_0 = \omega^{\rm p} \tag{14}$$

$$\mathscr{S}(\mathbf{k}^{\rm s}_\perp, \mathbf{k}^{\rm i}_{\perp 0}) = |\psi(\mathbf{k}^{\rm s}_\perp + \mathbf{k}^{\rm i}_\perp)|^2 = {\rm e}^{-(|\mathbf{k}^{\rm s}_\perp + \mathbf{k}^{\rm i}_{\perp 0}|^2 - \kappa_\perp)^2/\delta^2_{\kappa\perp}} \tag{15}$$

$$\mathscr{L}(\mathbf{k}^{\rm s}_\perp, \mathbf{k}^{\rm i}_{\perp 0}; \omega^{\rm s}, \omega^{\rm i}_0) = {\rm sinc}^2(L\,\Delta k_z/2). \tag{16}$$

In the paraxial regime the spatial structure of the photon pairs is directly inherited from the pump beam [15, 17, 19, 20, 24]. The use of a pump beam with a restricted BG structure in the azimuthal angle, $\varphi_0 \le \varphi_p \le \varphi_0 + \pi$, which corresponds to a half-plane obstruction, yields a CAS that for an idler photon with transverse wavevector $\mathbf{k}^{\rm i}_\perp$ results in signal photons with transverse wavevectors within a semicircle centered at $-\mathbf{k}^{\rm i}_\perp$. Nevertheless, for a non paraxial pump beam, the azimuthal asymmetry observed in the AS has a bearing on the observed CAS. Specifically, because the CAS is the result of multiplying the pump AS $\mathscr{S}(\mathbf{k}^{\rm s}_\perp, \mathbf{k}^{\rm i}_{\perp 0})$ by the function $\mathscr{L}(\mathbf{k}^{\rm s}_\perp, \mathbf{k}^{\rm i}_{\perp 0}; \omega^{\rm s}, \omega^{\rm i}_0)$ it becomes possible, particularly for large values of $\kappa_\perp$ or long crystals [25], for the latter function to act as a filter obscuring parts of the former. This can result in the CAS revealing only part of the full pump AS. This behavior depends on the selection of $\mathbf{k}^{\rm i}_\perp$, and exhibits a high sensitivity to small displacements of the fixed idler detector, as illustrated with specific simulations in the Appendix. In the Appendix we likewise illustrate the effect of the function $\mathscr{L}(\mathbf{k}^{\rm s}_\perp, \mathbf{k}^{\rm i}_{\perp 0}; \omega^{\rm s}, \omega^{\rm i}_0)$, for several half-plane obstruction orientations φ_p, in terms of limiting the extent of the CAS with respect the full pump AS. Individual plots of the functions $\mathscr{S}(\mathbf{k}^{\rm s}_\perp, \mathbf{k}^{\rm i}_{\perp 0})$ and $\mathscr{L}(\mathbf{k}^{\rm s}_\perp, \mathbf{k}^{\rm i}_{\perp 0}; \omega^{\rm s}, \omega^{\rm i}_0)$, as well as of their product, clarify this behavior.

Note that while the equations presented above assume that the SPDC photons are ideally monochromatic, the extension to a non-zero SPDC bandwidth is straightforward [26]. Such a non-zero emission bandwidth can have a significant effect on the spatial properties of the measured photon pairs, particularly on the AS and CAS functions. Since in practice an interference filter is used, the filter bandwidth represents an additional degree of freedom which can be used in order to shape the photon pair characteristics. In particular, summing over a range of SPDC frequencies leads to the tendency to suppress sharp features in the AS, resulting in regions of near-uniformity. In the following Section we present experimental results along with numerical simulations based on a version of our theory which does take into account a non-zero SPDC bandwidth.

IV. EXPERIMENT

Our setup is depicted in Figure 2. The SPDC source is based on a β barium borate (BBO) crystal, pumped by an apertured Bessel-Gauss beam.

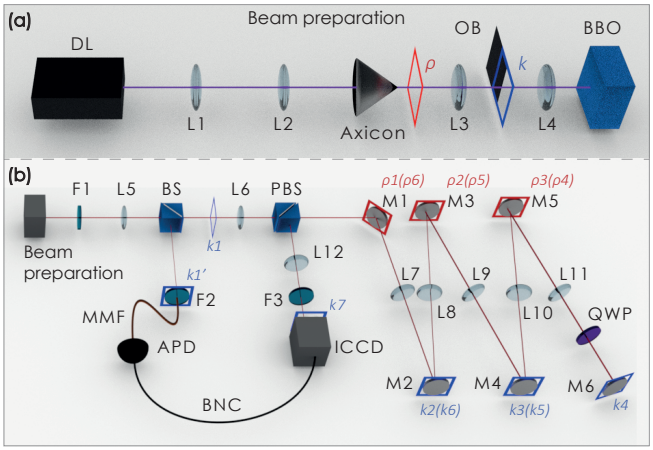

FIG. 2. Experimental setup. (a) Structured beam generation. (b) Optical delay and detection.

This structured pump is prepared as follows (see Figure 2(a)). The beam from a diode laser (DL), at $\lambda_{\rm p} = 405.5$ nm with output power of 100 mW is transmitted through a telescope built from lenses L1 and L2 with focal lengths $f_1 = 5$ cm and $f_2 = 15$ cm.

The resulting magnified beam, with diameter ~ 0.32 cm, illuminates an axicon, with apex angle of 1°. Our BG beam is in principle propagation invariant over a distance of 18 cm. A plane 4 cm ahead of the axicon tip is selected because it exhibits a high-quality BG intensity pattern, and is imaged onto the plane of the crystal through a $4f$ optical system, composed of lenses L3 and L4 with $f_3 = 20$ cm and $f_4 = 30$ cm as shown in Figure 2(a).

With this configuration, at the crystal plane, the zeroth-order BG beam is composed of concentric rings with an intensity maximum at the center; our corresponding experimental measurement is shown in Figure 3(a). In Figure 3(b) we show the experimentally-measured transverse intensity on the Fourier plane (labelled k). The observed intensity pattern represents the angular spectrum composed of an annulus with radius, in transverse momentum space, of $\kappa^{\rm p}_\perp$ and width $\delta_{\kappa\perp}$; in our specific case, $\kappa^{\rm p}_\perp = 0.170\mu{\rm m}^{-1}$ and $\delta_{\kappa\perp} = 0.0008\mu{\rm m}^{-1}$, as determined by a measurement with a CCD camera on plane k in Figure 2(a).

The apertured BG beam is obtained using a binary mask in the form of a half plane (OB) which can be rotated on the transverse plane, so that its edge coincides at all times with the center of the pump angular spectrum annulus. For illustration purposes, Figure 3(c) shows the experimentally-obtained apertured pump beam on the crystal plane for an orientation $\varphi_p = 135°$; it results in an angular spectrum in the form of the half-annulus shown in Figure 3(d).

For the following discussion we refer to the setup shown in Fig. 2(b). Photon pairs are produced through the process of SPDC in a BBO crystal of length 1 mm, cut at an angle of $\theta_c = 29.3°$ for type I phasematching (both signal and idler photons are horizontally-polarized ordi-

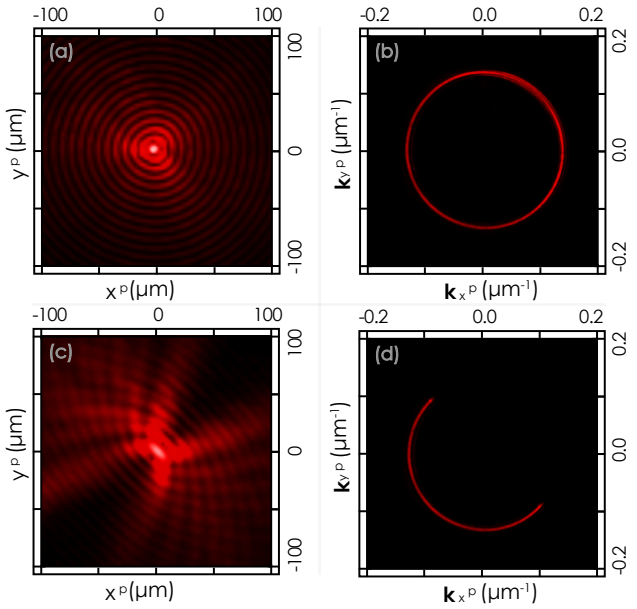

FIG. 3. Experimental measurements. (a) Transverse intensity of the unobstructed zeroth-order Bessel-Gauss pump beam. (b) Angular spectrum of the beam. (c) And (d) are similar to (a) and (b) for the specific case of the obstruction oriented at $\varphi_p = 135°$.

nary waves, while the pump is an extraordinary wave). A filter (F1) which transmits wavelengths $\lambda > 630$ nm is placed following the crystal, for pump suppression. A lens (L5) with $f_5 = 5$ cm, yields a Fourier plane labelled $k1$ on which the angular spectrum of the generated photons may be observed. The angular spectrum is measured with an intensified CDD camera (ICCD) placed on plane $k7$, which is equivalent to plane $k1$, as shown in Fig.1(a) along with their corresponding simulation in Fig.1(b). The observed angular spectrum is consistent with previous studies of SPDC utilizing a BG pump beam, and it reveals the expected two asymmetrically placed rings, one contained by the other. The space between the two rings also presents non-vanishing counts.

A beam splitter (BS) is placed prior to $k1$, resulting in a Fourier plane $k1'$ in the reflected arm (which is equivalent to $k1$). The photon pairs are split non-deterministically by the BS with a 50% probability. Following transmission through a 810 ± 5 nm bandpass filter (F2) for further pump and/or spurious photon suppression, we place on $k1'$ the tip of a multimode fiber (MMF) with core radius 50 μm to collect the idler photon. The fiber tip is mounted on a two-dimensional motor with a minimum step of 50 nm, as a consequence it can be set with high precision at an arbitrary location of the transverse plane, allowing a detailed characterization of the SPDC angular spectrum. This fiber leads to an avalanche photodiode (APD) that detects an idler photon on $k1'$ and heralds the presence of a signal-mode single photon which reaches $k1$.

The ICCD camera can be triggered by the electronic pulse produced upon detection of an idler photon by the APD. However, the electronic pulse is produced by the APD with a delay of 20 ns with respect to the time of photodetection, which is added to the insertion delay in the ICCD camera, of 19.9 ns. In order to compensate for the total optical and electronic delay and thus balance the signal and idler channel transit times, including the effects of the optical fiber and cable lengths, the signal photon is made to traverse an image-preserving optical delay line with total length of 18 m.

Proceeding with the delay line, at a distance of 40 cm from $k1$ we placed lens L6 ($f_6 = 40$ cm), generating the plane $\rho 1$ which constitutes an image of the crystal plane. Our optical delay was designed in a double-pass geometry. For this purpose, we set a polarizing beam splitter (PBS) at a distance of 40 cm from L6, through which the horizontally-polarized, single-mode signal photon is deterministically transmitted in the forward direction. Following reflection at mirror M1, placed following the PBS, the signal-mode single photon is transmitted through a series of 5 f-f optical systems, based on lenses L7-L11, with reflections at mirrors M2-M5. The first two lenses (L7 and L8) have focal lengths of 75 cm, while the remaining lenses (L9-L11) have focal lengths $f_9 = f_{10} = f_{11} = 100$ cm. Before the last mirror (M6) a quarter wave plate (QWP) is oriented so that in two passes the single-photon polarization flips from horizontal to vertical. The signal-mode single photon then traverses the 5 f-f optical systems once more in the backwards direction, reaching PBS again at which the now vertically-polarized signal photon is deterministically reflected.

Note that mirrors M2-M6 correspond, in an alternating fashion, to the transverse momentum and transverse position spaces. A label $k2(k6)$ next to M2 denotes that in the forward direction, the plane of this mirror corresponds to the second transverse momentum-coordinate plane (k) and in the backwards direction to the sixth. The label $\rho_2(\rho_5)$ similarly indicates the second (fifth) coordinate-space plane in the forward (backward) direction. In the setup figure, red-colored / blue-colored squares indicate transverse position / momentum planes.

In the backward-propagating direction the signal photon reaches plane $\rho 1$, also labelled $\rho 6$. Following reflection by PBS, the signal photon is transmitted through lens L12 with $f_{12} = 40$ cm placed one focal length distance from plane $\rho 6$, and through an 810 ± 5 nm bandpass filter (F3), for additional pump and/or spurious photon suppression. The ICCD camera is finally placed at a distance of f_{12} from lens L12; the plane of the camera is labelled as $k7$ in Figure 2(b).

V. RESULTS AND DISCUSSION

Our experimental data are illustrated in Figures 4 and 5. These results are organized as follows: each

row corresponds to a particular orientation φ_p of the pump half-annulus angular spectrum. Values $\varphi_p = 0°, 180°, 90°, 270°$ are included in Fig. 4, while $\varphi_p = 45°, 225°, 135°, 315°$ appear in Fig. 5. Additional orientations φ_p are presented in the Supplementary Information. In each of these two figures, the color bar indicates the relative intensity and the white dot represents the (MMF) fiber tip position, not to scale. The diameter of the fiber-tip with respect to the AS is indicated by the black dot near the left-bottom corner. The first column (i) corresponds to a measurement of the pump angular spectrum. The second column (ii) shows the measured SPDC signal-photon angular spectrum (AS). The third column (iii) shows the conditional angular spectrum (CAS) of the signal-mode single photon and the fourth column (iv) is a simulation corresponding to the experimental parameters in the second and third columns. In (iii), the detected coincident events between the APD in the idler channel and the triggered ICCD in the signal channel are shown. As in the second column, the fixed position of the idler-mode detector is indicated by a white dot. Coincidences were obtained by summing over 3600 accumulations, each with an exposure time of 1 s. Note that the idler detector position (white dot) and center of the measured CAS fulfill transverse momentum conservation. Note also that a 'halo' which corresponds in shape and position with the AS shown in the second column is visible; this halo is only observed when filter (F2) is removed and is composed of accidental coincident events, which however, are useful for placement of the CAS with respect to the SPDC AS. The white dot at the location with highest counts indicates the chosen position for the idler-photon detector. Note the excellent agreement between the simulations and the measurements.

It is instructive to compare the resulting AS and CAS of the SPDC photon pairs for the two cases $\varphi_p = 0°$ and $\varphi_p = 180°$, which correspond to the top half and bottom half of the unobstructed pump AS. It becomes clear that whereas the single-photon AS for the unobstructed pump is composed of two asymmetrically placed rings, the obstruction with $\varphi_p = 0°$ results in the SPDC AS largely only retaining the outer ring, while the obstruction with $\varphi_p = 180°$ results in the SPDC AS largely only retaining the inner ring. Note that this asymmetry in the vertical direction of the pump AS is governed by the pump walk-off parameter β and the orientation of the optic axis which for our source occurs along the vertical direction. For other obstruction orientations, the SPDC AS exhibits portions of both, the external and internal rings. The relative weight of these portions are balanced for the cases $\varphi_p = 90°$ and $\varphi_p = 270°$, and are less balanced for the remaining diagonal orientations, presented in the succeeding figure.

Our results highlight the possibility of controlling the SPDC emission characteristics through the type of obstruction applied to a BG beam pump. In particular, choosing to obstruct the bottom(top) half of the pump AS results in a wider(narrower) SPDC emission cone.

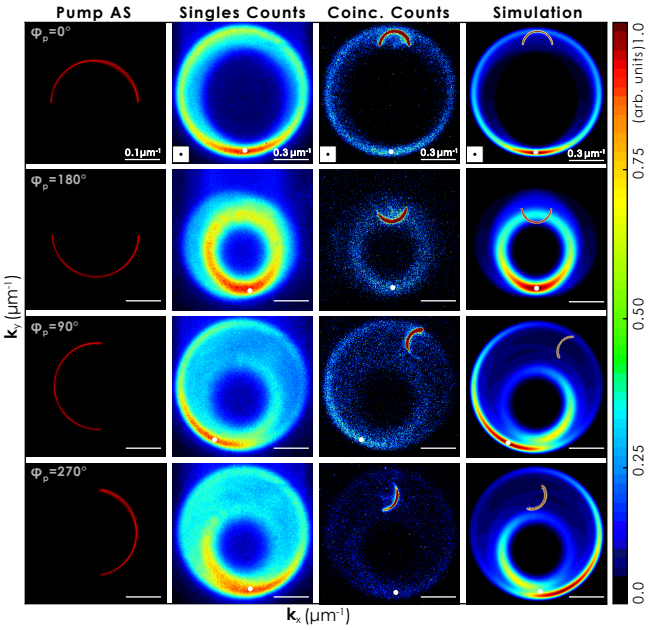

FIG. 4. Columns 1-3 correspond to measurements of (i) the pump AS, (ii) the resulting single-photon AS, and (iii) the resulting CAS with the idler detector. Column 4 presents the simulation of the SPDC single-photon AS and the CAS, for the same experimental situation as in columns 2 and 3. The four rows correspond to $\varphi_p = 0°$, 180°, 90°, and 270°, respectively.

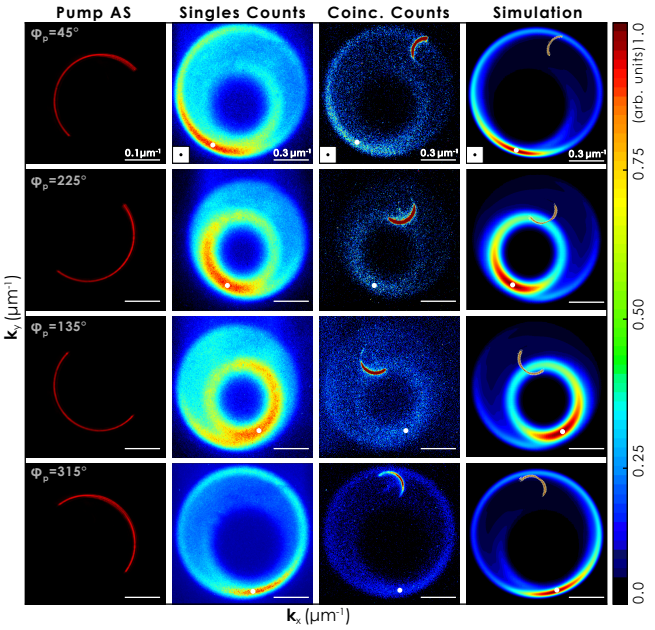

FIG. 5. This figure is presented in the same format as Fig. 4. In this case, the four rows correspond to the orientations $\varphi_p = 45°$, 225°, 135°, and 315°.

Note that the two rings, which appear simultaneously in the unobstructed pump case, meet tangentially at the bottom of each of the two rings. Let us concentrate on

the emission characteristics along the vertical direction, and label the lower portion of the AS where the two rings meet the idler mode, and the upper portion where the two rings differ angularly the signal mode. We could configure our source so that the external-ring portion of the signal mode reaches a distant observer O_1, while the internal-ring portion reaches a different distant observer O_2. An experimenter stationed at the source could then determine, according to the choice of obstruction of the pump AS, whether a single-mode signal photon heralded by the detection of an idler photon reaches O_1 or O_2, or whether it can reach either of the two observers with controllable probabilities.

VI. CONCLUSIONS

We have studied, from both theoretical and experimental perspectives, the spatial properties of photon pairs produced by the process of spontaneous parametric down-conversion (SPDC) with an apertured, zeroth-order Bessel-Gauss pump beam. We have concentrated on frequency-degenerate, co-polarized (i.e. type-I) SPDC with a binary aperture applied to the the pump angular spectrum in the form of a half-plane with its edge tangent to the pump axis. Using such an aperture we are able to control the resulting SPDC spatial properties in the following sense: while the SPDC angular spectrum for an unobstructed zeroth-order BG beam is in the form of two non-concentric cones asymmetrically placed on the transverse plane, the obstruction allows us to select either one of the cones in the dual-cone SPDC angular spectrum, or a portion of both depending on the angular orientation of the binary obstruction. From this selection we can also control the properties of the conditional angular spectrum.

A key advantage of the method proposed and demonstrated here, is that despite any complexity in setting up the structured pump beam (for example involving the use of an axicon, as in this work, or active elements such as spatial light modulators), the resulting properties of the SPDC photon pairs can be effectively modified through easily-implemented pump obstructions. Importantly, such modifications can be applied efficiently and in real time as needed, since the placement and displacement/rotation of obstructions does not lead to the need for re-aligning the setup. While we believe that this type of straightforward control of the SPDC emission properties could prove particularly well-suited for setting up large alphabets for quantum communications, it could be useful as a general tool for quantum information processing protocols.

ACKNOWLEDGMENTS

This work was supported by CONACYT LN-293471, México, by PAPIIT(UNAM) grant IN1050915, and by AFOSR grant FA9550-16-1-0458.

VII. APPENDIX

The purpose of this appendix is to present some additional details regarding the behavior of the conditional angular spectrum (CAS). We wish first to illustrate the high degree of sensitivity of the CAS to the location of the idler detector. For the specific case of the half-plane aperture oriented at $\varphi_p = 135°$, Fig. 6 shows the effect of a slight radial displacement of the position of the idler detector. Panel (a) shows a simulation of the SDPC angular spectrum with three white dots, labelled A, B, and C, each indicating a particular position of the idler detector; note that location B is identical to the situation shown in the third row of Fig. 5. The array of nine panels (b-j) on the right is organized as follows: while the three rows correspond to the the three locations for the fixed idler detector A, B, and C, the three columns correspond to plots of functions $\mathscr{S}(\mathbf{k}^{\mathrm{s}}_{\perp}, \mathbf{k}^{\mathrm{i}}_{\perp 0})$, $\mathscr{L}(\mathbf{k}^{\mathrm{s}}_{\perp}, \mathbf{k}^{\mathrm{i}}_{\perp 0}; \omega^{\mathrm{s}}, \omega^{\mathrm{i}}_0)$ and the product of the latter two, respectively. Note, that the CAS differs appreciably amongst the three situations shown. While in all cases parts of the pump AS are concealed in the resulting CAS, the extent and type of this concealment is different in the three cases: A shows more concealment as compared to B, and C shows fragmentation, in addition to concealment.

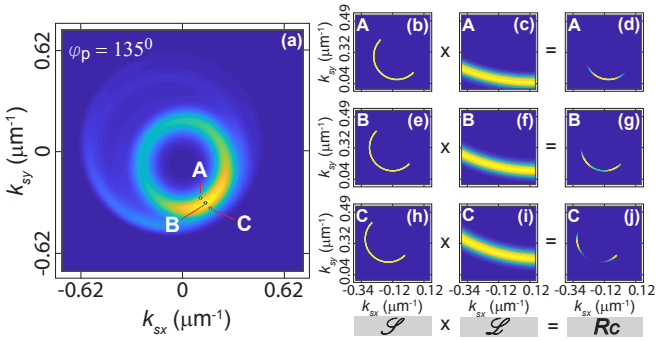

FIG. 6. (a): Simulated SPDC AS for $\varphi_p = 135°$. (b-j): array of nine panels shows plots of functions $\mathscr{S}(\mathbf{k}^{\mathrm{s}}_{\perp}, \mathbf{k}^{\mathrm{i}}_{\perp 0})$, $\mathrm{L}(\mathrm{k}^{\mathrm{s}}_{\perp}, \mathbf{k}^{\mathrm{i}}_{\perp 0}; \omega^{\mathrm{s}}, \omega^{\mathrm{i}}_0)$, and $\mathrm{S}(\mathrm{k}^{\mathrm{s}}_{\perp}, \mathbf{k}^{\mathrm{i}}_{\perp 0})\mathscr{L}(\mathbf{k}^{\mathrm{s}}_{\perp}, \mathbf{k}^{\mathrm{i}}_{\perp 0}; \omega^{\mathrm{s}}, \omega^{\mathrm{i}}_0)$ for the three idler detector positions A,B, C identified in panel (a) .

In Fig. 7 we show the behavior of the CAS and its constituent functions $\mathscr{S}(\mathbf{k}^{\mathrm{s}}_{\perp}, \mathbf{k}^{\mathrm{i}}_{\perp 0})$ and $\mathscr{L}(\mathbf{k}^{\mathrm{s}}_{\perp}, \mathbf{k}^{\mathrm{i}}_{\perp 0}; \omega^{\mathrm{s}}, \omega^{\mathrm{i}}_0)$ in response to the variation of the orientation of the half-plane obstruction, φ_p. The figure is organized as follows: the 5 rows correspond to the following obstruction orientations $\varphi = 0°$, $\varphi = 45°$, $\varphi = 90°$, $\varphi = 135°$, and $\varphi = 180°$, respectively. The three columns correspond to plots of the functions $\mathscr{S}(\mathbf{k}^{\mathrm{s}}_{\perp}, \mathbf{k}^{\mathrm{i}}_{\perp 0})$, $\mathscr{L}(\mathbf{k}^{\mathrm{s}}_{\perp}, \mathbf{k}^{\mathrm{i}}_{\perp 0}; \omega^{\mathrm{s}}, \omega^{\mathrm{i}}_0)$, and $\mathscr{S}(\mathbf{k}^{\mathrm{s}}_{\perp}, \mathbf{k}^{\mathrm{i}}_{\perp 0})\mathscr{L}(\mathbf{k}^{\mathrm{s}}_{\perp}, \mathbf{k}^{\mathrm{i}}_{\perp 0}; \omega^{\mathrm{s}}, \omega^{\mathrm{i}}_0)$. Note that the degree of concealment of the pump AS in the resulting CAS depends on φ_p; for example, $\varphi = 90°$ exhibits considerably more concealment than $\varphi = 0°$.

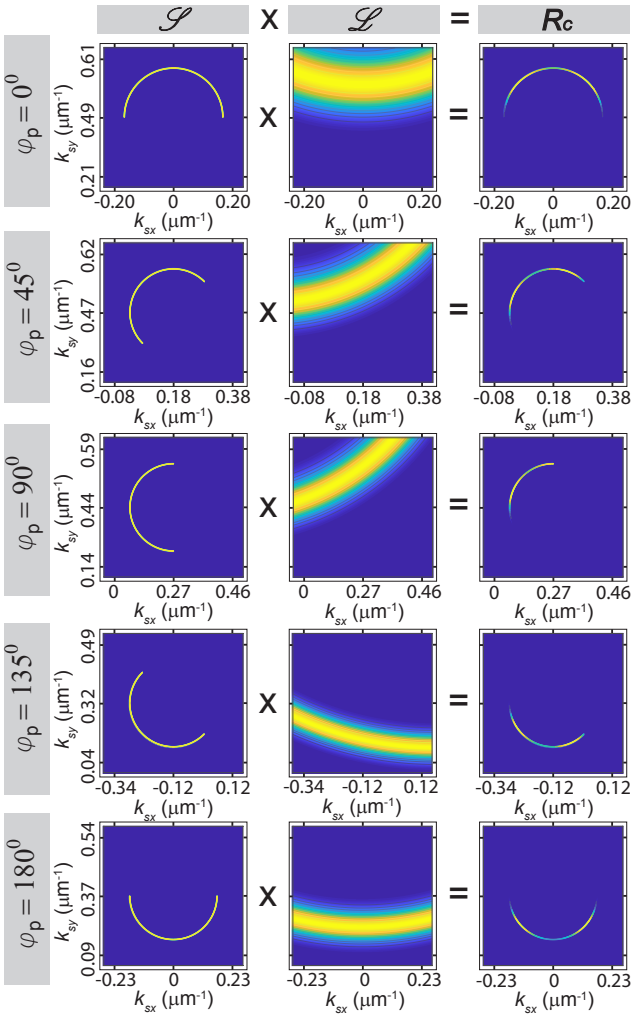

FIG. 7. Plots of the functions $\mathscr{S}(\mathbf{k}^{\mathrm{s}}_{\perp}, \mathbf{k}^{\mathrm{i}}_{\perp 0})$, $\mathscr{L}(\mathbf{k}^{\mathrm{s}}_{\perp}, \mathbf{k}^{\mathrm{i}}_{\perp 0}; \omega^{\mathrm{s}}, \omega^{\mathrm{i}}_{0})$, and $\mathscr{S}(\mathbf{k}^{\mathrm{s}}_{\perp}, \mathbf{k}^{\mathrm{i}}_{\perp 0})\mathscr{L}(\mathbf{k}^{\mathrm{s}}_{\perp}, \mathbf{k}^{\mathrm{i}}_{\perp 0}; \omega^{\mathrm{s}}, \omega^{\mathrm{i}}_{0})$, in each of the three columns, respectively, for the following obstruction orientations: $\varphi_p = 0^\circ, 45^\circ, 90^\circ, 135^\circ, 180^\circ$, in each of the five rows, respectively.

[1] X. Liu, Q. Li, A. Sikora, M. Sentis, O. Utéza, R. Stoian, W. Zhao, G. Cheng, and N. Sanne, *Truncated Gaussian-Bessel beams for short-pulse processing of small-aspect-ratio micro-channels in dielectrics*, Opt. Exp. **27**, 6996 (2019).

[2] Turquet, X. Zang, J.-P. Kakko, H. Lipsanen, G. Bautista, and M. Kauranen, *Demonstration of longitudinally polarized optical needles*, Opt. Exp. **26**, 27572 (2018).

[3] P. Jones, O. Marago, and G. Volpe, *Optical Tweezers*, Cambridge University Press, Cambridge (2015).

[4] M. Mirhosseini, O. S. Magaña-Loaiza, M. N. O'Sullivan, B.Rodenburg, M. Malik, M.P. J. Lavery, M. J. Padgett, D. J. Gauthier, and R. W. Boyd, *High-dimensional quantum cryptography with twisted light*, New J. Phys. **17**, 033033 (2015).

[5] A. Classen, J. von Zanthier, M.O. Scully, and G.S. Agarwal, *Superresolution via structured illumination quantum correlation microscopy*, Optica **4** 580-587 (2017).

[6] R. Jáuregui and J. P. Torres, *On the use of structured light in nonlinear optics studies of the symmetry group of a crystal*, Sci. Rep. **6**, 20906 (2016).

[7] J. C. Gutierrez-Vega and M. A. Bandres, *Helmholtz-Gauss waves*, J. Opt. Soc. Am. A **22**, 289-298 (2005).

[8] Z. Bouchal, J. Wagner, and M. Chlup, *Self-reconstruction of a distorted non-diffracting beam*, Opt. Comm. **151**, 207211 (1998).

[9] M. McLaren, T. Mhlanga, M.J. Padgett, F.S. Roux and A. Forbes, *Self-healing of quantum entanglement after an obstruction*, Nat. Comm. **5**, 3248 (2014).

[10] G. Gbur and O. Korotkova, *Angular spectrum representation for the propagation of arbitrary coherent and partially coherent beams through atmospheric turbulence*, J.

Opt. Soc. Am. A **24**, 745752 (2007).

[11] A.H. Ibrahim, F.S. Roux, M. McLaren, T. Konrad, and A. Forbes, *Orbital-angular-momentum entanglement in turbulence* Phys. Rev. A **88**, 012312 (2013).

[12] A. Mair, A. Vaziri, G. Weihs, and A. Zeilinger, *Entanglement of the orbital angular momentum states* of photons," Nature **412**, 313 (2001).

[13] G. Molina-Terriza, J.P. Torres and L. Torner, *Twisted photons*,' Nat. Phys. **3**, 305 (2007)

[14] M. McLaren, M. Agnew, J. Leach, F.S. Roux, M.J. Padgett, R.W. Boyd, and A. Forbes, *Entangled Bessel-Gaussian beams*, Opt. Exp.**20** 23589 (2012).

[15] H. Cruz-Ramírez, R. Ramírez-Alarcón, F. J. Morelos, P. A. Quinto-Su, J. C. Gutíerrez-Vega, and A. B. U'Ren, *Observation of non-diffracting behavior at the single photon level*, Opt. Exp. **20**, 29761 (2012).

[16] V. Vicuña-Hernández, H. Cruz-Ramírez, R. Ramírez-Alarcón, and A. B. U'Ren, *Classical to quantum transfer of optical vortices*, Opt. Exp. **22**, 20027 (2014).

[17] Y. Jeronimo-Moreno and R. Jauregui, *On demand generation of propagation invariant photons with orbital angular*, Phys. Rev. A **90**, 013833 (2014).

[18] C.L. Hernandez-Cedillo and R. Jauregui *Spin and orbital angular momentum correlations in parametric downconversion of Bessel beams*, J. Opt. **13**, 064021 (2011).

[19] S. Prabhakar, S. G. Reddy, A. Aadhi, A. Kumar, P. Chithrabhanu, G. K. Samanta, and R. P. Singh, *Spatial distribution of spontaneous parametric down-converted photons for higher order optical vortices*, Opt. Comm. **326**, 64-69 (2014).

[20] M. V. Jabir, N. A. Chaitanya, A. Aadhi, and G. K. Samanta, *Generation of "perfect" vortex of variable size and its effect in angular spectrum of the down-converted photons*, Sci. Rep. **6**, 21877 (2016).

[21] A. Anwar, P. Vaity, C. Perumangatt, and R. P. Singh, *Direct transfer of pump amplitude to parametric down-converted photons* Opt. Lett. **43**, 1155 (2018).

[22] V. Vicuña-Hernández, J. T. Santiago,Y. Jerónimo-Moreno, H. Cruz-Ramírez, R. Ramírez-Alarcón, A.B. U'Ren and R. Jáuregui, *Double transverse wave-vector correlations in photon pairs generated by spontaneous parametric down-conversion pumped by Bessel-Gauss beams*, Phys. Rev. A **94**, 063863 (2016).

[23] Y. Jeronimo-Moreno and R. Jauregui *Type I parametric down conversion of highly focused Gaussian beams in finite length crystals*, J. Opt. **16**,065201(2014).

[24] C. H. Monken, P. H. S. Ribeiro, and S. Pádua, *Transfer of angular spectrum and image formation in spontaneous parametric down-conversion*, Phys. Rev. A **57**, 3123 (1998).

[25] R. Ramírez-Alarcón, H. Cruz-Ramírez and A.B. U'Ren, *Effects of crystal length on the angular spectrum of spontaneous parametric downconversion photon pairs*, Laser Phys. **23**, 055204 (2013).

[26] R. Ramírez-Alarcón, V. Vicuña-Hernández, H. Cruz-Ramírez and A. B. U'Ren, *Transverse amplitude transfer experiments based on the process of spontaneous parametric downconversion*, Phys. Scr. **90**, (2015).